Computational Materials Science 78 (2013) 116–122

Contents lists available at SciVerse ScienceDirect

Computational Materials Science

journal homepage: www.elsevier.com/locate/commatsci

Effects of aluminum diffusion on the adhesive behavior of the Ni(1 1 1)/Cr_2O_3(0 0 0 1) interface: First principle study

Liu Hui [a,b], Li Yuping [a,b], Zhang Caili [a,b], Dong Nan [a,b], Lan Aidong [a,b], Li HongFei [a,b], Dong Hongbiao [b,c], Han Peide [a,b,*]

[a] College of Materials Science and Engineering, Taiyuan University of Technology, No. 79, Yingze Street, Wanbolin District, Taiyuan 030024, China
[b] Key Laboratory of Interface Science and Engineering in Advanced Materials, Taiyuan University of Technology, Ministry of Education, Taiyuan 030024, China
[c] Department of Engineering, University of Leicester, Leicester LE1 7RH, UK

ARTICLE INFO

Article history:
Received 22 April 2013
Received in revised form 21 May 2013
Accepted 23 May 2013
Available online 21 June 2013

Keywords:
First-principles
Oxidation
Interface
Diffusion
Nickel alloy

ABSTRACT

Density functional theory was employed to investigate the structure and properties of Ni/Cr_2O_3 and Ni/Al_2O_3/Cr_2O_3. The O-terminated Ni(1 1 1)/Cr_2O_3(0 0 0 1) interface was firstly found to be the most stable configuration. Based on this construction, the effects of the Al diffusion at the Ni/Cr_2O_3 interface were further studied. The results of total energies indicate that Al atoms originating from Ni slab prefer to diffuse into Cr_2O_3 slab through the interface, resulting in the formation of alumina at the Ni/Cr_2O_3 interface. Due to the presence of Al atoms, there was an amazing increase in the work of adhesion, whereas the Ni/Al_2O_3/Cr_2O_3 interface showed the strongest stability. Moreover, this calculated work well agrees with the reported experimental results.

1. Introduction

Nickel based superalloys are widely used in gas turbine engines, steam generator tubes and solid oxide fuel cells, owing to its excellent oxidation and corrosion resistances and high strength-to-weight ratio. For applications in oxygen-rich environments at very high temperatures, Ni based alloys rely on the formation of protective thermally grown oxide (TGO) scale extending service life, which inspires us to develop a better understanding of the oxidation. In recent years, a lot of researches have been carried out to clarify the components and structures of complicated oxides formed on Ni based alloys. Previous studies [1–3] on the oxidation of NiCoCrAlY alloy have showed that the TGO mainly consists of Al_2O_3, Cr_2O_3, $NiCr_2O_4$, $NiAl_2O_4$ and NiO, and that spinel $NiCr_2O_4$/$NiAl_2O_4$ normally forms between Al_2O_3/Cr_2O_3 and NiO through a solid state reaction during oxidation. Morphologies, microstructures and chemical composition of oxide films grown on Ni based alloys in oxygenated high temperature water were also investigated [4,5]. Although evolution processes of the layer oxide proposed were different, Hu et al. [6], Gigins and Pettit [7] and Nijam et al. [8] predicted the same mature oxide structure grown on NiCrAl alloys: an outer NiO layer at the oxide/gas interface, an inner Cr_2O_3 layer, and an Al_2O_3 layer at the oxide/alloy interface. Similar with the above deduction, the same multilayer oxides also has been found in two Ni based superalloys, SRR99 and CMSX10N [9]. In addition, G.Y. Laing pronounced that the lattice mismatch between Cr_2O_3 and Ni is less than that between Al_2O_3 and Ni, which implies that Cr_2O_3 is easier to nucleate and grow than Al_2O_3 during the early stage of oxidation process [3]. Generally, the TGO grows on alloys because of the inward diffusion of oxygen and the outward diffusion of metal atoms. Thus it is worthwhile studying the construction of multilayer oxides to explain the diffusion sequences of different metal atoms.

By virtue of the development of density-functional theory (DFT) and efficient computational schemes coupled with advanced computer power, the first-principles calculations of oxide/metal interfaces have contributed a lot in revealing the bonding nature and adhesion mechanism at interfaces [10–17]. One of the impressive findings is significant effects of stoichiometry, namely termination species of oxide surfaces, showing that different interface stoichiometry induces different adhesive energies and properties with various charge transfer and orbital hybridization. The atomic structure characterization of the Metal(1 1 1)/Al_2O_3(0 0 0 1) interfaces, where metal are FCC metals (Ni, Al, Ag, and Cu), was discussed with

* Corresponding author at: College of Materials Science and Engineering, Taiyuan University of Technology, No. 79, Yingze Street, Wanbolin District, Taiyuan 030024, China. Tel./fax: +86 351 6010311.
E-mail addresses: hanpeide@126.com, hanpeide@tyut.edu.cn (H. Peide).

0927-0256
http://dx.doi.org/10.1016/j.commatsci.2013.05.037

three possible oxide surface terminations by first principle calculations. It has been proposed that work of separation at the O-terminated metal/Al_2O_3 is several times larger than the Al-terminated and Al_2-terminated interface [10–13]. Similarly, Xiao et al. investigated O-terminated Cu/Cr_2O_3 interfaces with different interfacial configurations [14]. The effects of individual S and alloying elements on the interfacial adhesion and possible synergistic effect of co-doping were studied using DFT calculations [15,16]. Furthermore, the bilateral diffusion of atoms has been discussed [17]. Sun has researched the $Cr_2O_3(0001)$ surface with a partially or totally Al-substituted external layer, which implies the formation of Cr_2O_3/Al_2O_3 interface [18]. In our previous studies, a multilayer structure with Si enrichment at the Fe–Cr(Si)/FeO interface was evaluated [19]. However, studies on the structure with Al enrichment at the Ni/(Al_2O_3)/Cr_2O_3 interface have not been reported as yet which is important for the oxidation in Ni based alloys. Thus we carried out these investigations by using first-principles calculations and reported the results in this paper.

2. Theoretical method

The plane wave pseudopotential method [20] and Local Density Approximation (LDA) were implemented in the CASTEP code (Cambridge Sequential Total Energy Package). LDA with Ceperley–Alder–Perdew–Zunger (CAPZ) functional [21,22] was employed as exchange–correlation functional. Ground state atomic geometries were determined by minimizing the Hellman–Feynman forces. The Brillouin zone was sampled with Monkhorst–Pack *k*-point grid [23]. For the slab, a [3 × 3 × 1] *k*-point mesh was used. The plane-wave cutoff in our calculations was 340 eV. This set of parameters assured the convergence tolerance of energy of 1.0×10^{-5} eV/atom, maximum force of 0.03 eV/Å, and maximum displacement of 1.0×10^{-3} Å in the calculations.

To validate the method, the lattice constants of Ni were calculated. Compared with the calculated value of 3.51 Å [24] and experimental value of 3.521 Å [25], our obtained crystal lattice constants of Ni are: $a = b = c = 3.46$ Å, and the good agreement thereby validates the application of the methodology to study the interfacial adhesion and diffusion.

3. Results and discussion

3.1. Surface structure and energy of Cr_2O_3

For the hexagonal unit cell, the atoms are stacked along the (0001) direction according to the sequence R-$CrCrO_3$–$CrCrO_3$-R, where R represents the continuing sequence in the bulk. In the corundum structure (0001) stacking sequence, there are three unique stoichiometric slice planes, such as O-terminated (O-rich), Cr-terminated (stoichiometric), and Cr_2-terminated (Cr-rich) [26]. In this work, the calculated surface energy of Cr-terminated $Cr_2O_3(0001)$ is 2.40 J/m^2, in agreement with available theoretical value of 2.95 [27] and 2.91 [28] J/m^2, which was obtained by Sun and Wysocki using Hartree–Fock LCAO (linear combination of atomic orbitals) program and Vienna ab initio simulation program (VASP). The calculated surface energy of O-terminated and Cr_2-terminated $Cr_2O_3(0001)$ surfaces are 3.11 and 2.97 J/m^2, respectively. For the (0001) surface of chromia, oxygen-terminated surface has a very unfavorable energy implying its instability, while Cr-terminated surface is surprisingly stable [26,28], that is similar to the stability of different stoichiometry $Al_2O_3(0001)$ surfaces [29,30]. It is important to note that although the stoichiometric $Cr_2O_3(0001)$ surface is stable relative to the O-terminated surface, interface formation with metal can reverse the stability, consistent with the alteration of metal/Al_2O_3 interface [13,30]. The calculated results for the three stoichiometry Cr_2O_3 surfaces elucidated that the O-terminated surface is the most instable structure, suggesting that the O-terminated metal/chromia interface should be the most energetically stable configuration. Our calculated surface energy of Ni(1 1 1) is 2.75 J/m^2, a slight different from the calculated results obtained by other method, i.e. 2.00 [11] and 2.69 [31] J/m^2 for VASP GGA (general gradient approximation) and Green-function LMTO (linear-muffin-tin-orbitals), respectively. However, all these calculated results are in good agreement with the experimentally measured values (2.38 J/m^2 [32], 2.45 J/m^2 [33]).

3.2. Interface structure of Ni/Cr_2O_3

The system containing 31 atoms with the crystalline orientation of the close-packed Ni(1 1 1)/[1 −1 0] parallel to that of

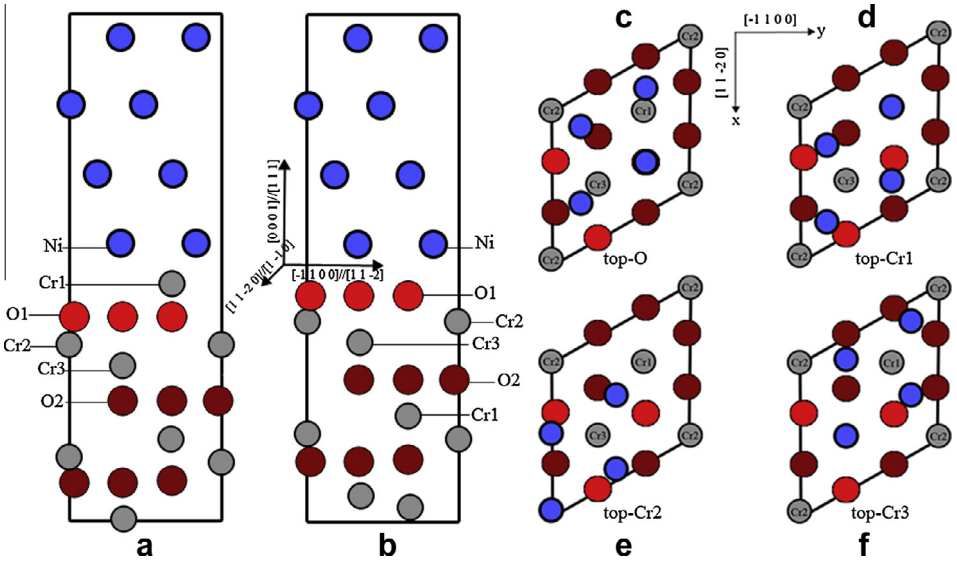

Fig. 1. Side view of (a) the Cr-terminated and (b) the O-terminated Ni(1 1 1)/Cr_2O_3(0001) interface model. Top view of four interface configurations with O-terminated: (c) top-O site, (d) top-Cr1 site, (e) top-Cr2 site, and (f) top-Cr3 site. For clarity, only the interfacial Ni layer in the top view is shown. Blue spheres represent Ni atoms, gray spheres are Cr atoms, and bright red spheres correspond to O atoms which are the closest to interface, dark red spheres to O atoms in the Cr_2O_3 bulk. (For interpretation of the references to color in this figure legend, the reader is referred to the web version of this article.)

Table 1
Total energies (eV) and work of adhesion (J/m^2) of the five Ni/Cr_2O_3 configurations in Fig. 1.

Interface	E_{tot} (eV)	W_{ad} (J/m^2)
O-terminated		
Top-O	−40307.9685	1.49
Top-Cr_1	−40307.9660	1.48
Top-Cr_2	−40307.8233	1.43
Top-Cr_3	−40307.9682	1.49
Cr-terminated		
Top-Cr	−40307.1013	0.80

Table 2
Total energies (eV), heat of segregation (eV) and work of adhesion (J/m^2) of the interfaces with different aluminum diffusion sites and coverage.

Construction	E_{tot} (eV)	ΔE_{seg} (eV)	W_{ad} (J/m^2)
Model *a* (clean interface)	−40307.9685	–	1.49
Model *b* (one Al in Ni)	−39018.5850	−0.0491	1.72
Model *c* (one Al on interface)	−39018.5886	−0.0527	1.68
Model *d* (one Al in Cr_2O_3)	−39019.6434	−1.1075	1.79
Model *e* (two Al in Cr_2O_3)	−37731.5271	−1.2119	2.53

$Cr_2O_3(0001)/[11-20]$ was adopted in this simulation. To simplify the model, we dealt with the Cr-terminated (stoichiometric) and O-terminated (O-rich) Ni(111)/Cr_2O_3(0001) interfaces shown in Fig. 1a and b, in which we maintain superlattice geometry of a four-layer slab of Ni(111) placed on the Cr_2O_3 slab. For the stoichiometric Ni/Cr_2O_3 interface, the Cr_2O_3 slab contains three O atomic layers and six Cr atomic layers, and for the O-terminated case, the top Cr layer of the slab is removed. Since there was a substantial amount of lattice mismatch (0.5%) between Ni and Cr_2O_3, we took average lattice constants of Ni slab and Cr_2O_3 slab as interface lattice constants. Then the supercell area was calculated as 0.2140 nm^2. Considering the atomic matching of two phases, lots of constructions in the interface model were expected. However, after relaxation, most of them converged into the same structure. Therefore, by adopting the adhesion energy criterion, for the O-terminated interface, we chose four typical high-symmetry constructions as shown in Fig. 1c–f: Ni above O atom (top-O), Ni above Cr1 atom (top-Cr1), Ni above Cr2 atom (top-Cr2), Ni above Cr3 atom (top-Cr3 or hollow).

Adhesion energies were then calculated for all geometries after allowing for atomic relaxations. The ideal work of adhesion, W_{ad} defined as the reversible work that is needed to separate an interface into two free surfaces in a theoretical experiment, characterizing the strength of the metal/ceramic interface [34], was calculated by the difference in the total energies between the interface and its isolated slabs:

$$W_{ad} = \left(E_X^{tot} + E_Y^{tot} - E_{X/Y}^{tot}\right)/A \quad (1)$$

here E_X^{tot} and E_Y^{tot} are the total energy of the relaxed, isolated Ni and Cr_2O_3 slabs in the same supercell when one of the slab is retained and the other is replaced by a vacuum, respectively. $E_{X/Y}^{tot}$ is the total energy of the Ni/Cr_2O_3 interface system. A is the total interface area of the unit cell. In general, the experimental cleavage energy values will always exceed W_{ad} because of plasticity and diffusion. The larger W_{ad} is, the larger the energy required for cleavage is. Hence, work of adhesion provides a useful quantity which is readily accessible by theoretical calculations or simulation.

Table 1 shows the total energies of the relaxed interfaces. It is clearly seen from the table that total energy of four different O-terminated Ni/Cr_2O_3 interfaces are consistently smaller than that of the Cr-terminated one, while the W_{ad} values obtained from four different O-terminated Ni/Cr_2O_3 configurations are almost twice of that of the Cr-terminated one, suggesting that O-terminated interface is energetically favorable. Similar simulations were reported for the adhesion of different stoichiometry metal/Al_2O_3 interfaces [10–13]. This discrepancy of adhesion work value can be attributed to the weak hybridization and negligible interfacial charge transfer of the Cr(Al)-terminated, as compared to strong ionic–covalent interactions and significant charge transfer of the O-terminated interface. In addition, since very little difference are found between 'top-O' and 'top-Cr1/top-Cr3' constructions, 'top-O' configuration was chosen as our initial Ni(111)/Cr_2O_3(0001) interface structure in the subsequent calculations.

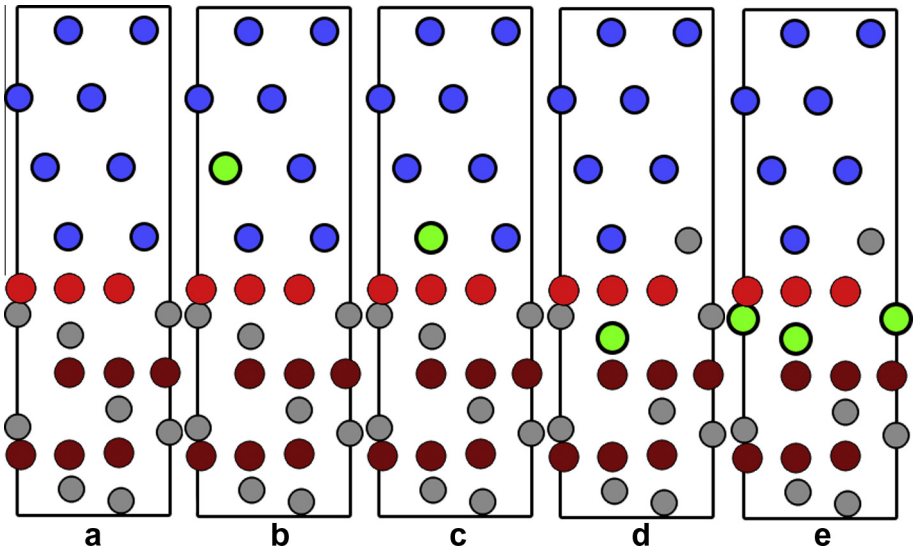

Fig. 2. (a) Structure of clean Ni/Cr_2O_3 interface without Al atom. (b) Structure of interface with an Al atom replacing a Ni atom in the Ni bulk. (c) Structure of interface with an Al atom supplying a Ni atom on the interface. (d) Structure of interface with an Al atom substituting a Cr atom close to the interface. (e) Structure of interface with two Al atoms substituting Cr atoms. The green spheres stand for Al atoms, blue spheres represent Ni atoms, gray spheres are Cr atoms, and bright red spheres correspond to O atoms close to interface, dark red spheres to O atoms in the Cr_2O_3 bulk. (For interpretation of the references to color in this figure legend, the reader is referred to the web version of this article.)

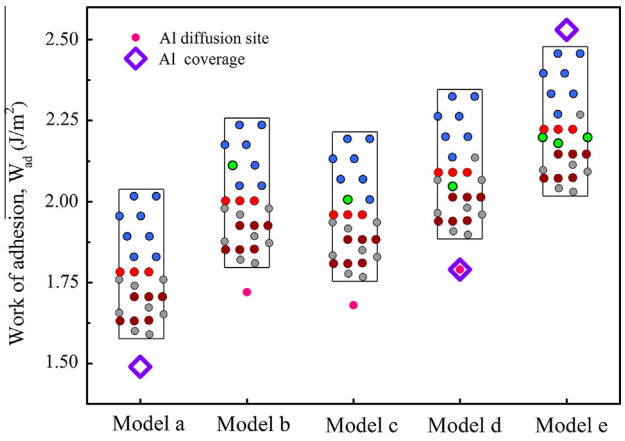

Fig. 3. Work of adhesion as a function of different aluminum diffusion sites and coverage.

3.3. Ni/Cr_2O_3 interface with Al

Based on the so-called 'top-O' construction, we attempted to provide information relative to the diffusion of Al atom from Ni into Cr_2O_3 bulk. To examine aluminum migration, we introduced aluminum at the different sites of the interface in the following way: firstly, the Al atom occupied Ni-substitutional site far away from the interface as shown in Fig. 2b, which indicated that the Al atom emanated from the Ni bulk. Next, the Al atom moved to the interface by replacing a Ni atom which was the closest to interface (Fig. 2c). Finally, to represent the Al diffusion into Cr_2O_3 bulk, we investigated the Ni/Cr_2O_3 interface with the Al substitution for a Cr atom close to the interface (Fig. 2d). The diffusion effect of Al on the structure and properties of Ni/Cr_2O_3 mainly comes from the interactions of the aluminum with its neighbors. To investigate the diffusion mechanism, the heat of segregation is defined in Eq. (2) [35].

$$\Delta E_{seg} = \frac{1}{n}\left(E_{Ni/Cr_2O_3:nAl} - E_{Ni/Cr_2O_3} + n \cdot E_{Ni} - n \cdot E_{Al}\right) \quad (2)$$

where $E_{Ni/Cr_2O_3:nAl}$ and E_{Ni/Cr_2O_3} are total energies of interface with and without aluminums, respectively. E_{Ni} and E_{Al} are the energies of Ni and Al atom, n is the number of Al atoms.

Table 2 lists the calculated total energies, heat of segregation and adhesion energies of five configurations with different diffusion sites and coverage of Al atoms. By comparing the total energies, we found that, in terms of energy, replacing a Cr atom in Cr_2O_3 slab is the most likely aluminum diffusion site with total energy of −39019.6434 eV. The values of heat of segregation also imply that Al atoms participating into the Cr_2O_3 slab is the most energetically stable diffusion site.

To reveal the impacts of aluminum diffusion sites and concentration on the interfacial properties, the work of adhesion illustrated in Fig. 3 was examined. It is interesting to find that, for an aluminum atom, no matter which diffusion site aluminum occupies, the adhesion of interface is improved compared with that of clean interface. Especially, the substitution of an Al atom for a Cr atom can enhance the interfacial adhesive work by the most encouraging increase of 0.3 J/m^2.

In these calculations, Cr atoms in the Cr_2O_3 slab were gradually substituted with Al atoms. As shown in Fig. 2a, d, and e, the coverage of 0, 50%, 100% for Al doped was calculated as well. For the clean interface, we got the work of adhesion (1.49 J/m^2) by employing the 'top-O' O-terminated mode. Inserting an Al atom into Ni/Cr_2O_3 supercell gives 50% coverage of aluminum, we demonstrated that the presence of aluminum can increase the interfacial strength to 1.79 J/m^2. The calculated result (2.53 J/m^2) with Al coverage of 100% was obtained by substituting two Cr atoms both of which are close to interface. In all, we can naturally affirm that the presence of Al atom remarkably enhanced the work of adhesion. Besides that, the more Al atoms diffuse, the better interfacial adhesion is. Moreover, it is worthy pointing out that the structure of interface with 100% Al coverage supports the formation of $Ni/Al_2O_3/Cr_2O_3$ multilayer oxide. Because both Al_2O_3 and Cr_2O_3 have the same structure with hexagonal close-packed (0001) layers of O atoms and two thirds of the octahedral holes filled by Al(Cr) atoms. As the increase of Al substitution, the top layer chromia turn out to be alumina though there is a small lattice mismatch between Al_2O_3 and Cr_2O_3.

These phenomena hint that though the Ni/Cr_2O_3 interface Al atoms stemming from Ni slab prefer to occupy Cr-substitutional sites, and that aluminum atoms can easily be incorporated into the (0001) chromia slab for any coverage. As known to all, both Al_2O_3 and Cr_2O_3 having the corundum-type structure (space group R3c), taking this into consideration, we can safely assume that Al atoms concentrate at the nickel/chromia interface must result in the formation of alumina between nickel and chromia, helping the presence of $Ni/Al_2O_3/Cr_2O_3$ construction. In fact, previous experimental investigations into the oxidation of Ni based alloys have reported the three-layer structure formation of an externally oxidized chromia and internal alumina, with Al_2O_3 being the layer next to the unoxidized substrate [6–9]. Recently, it has also been studied that alumina can grow on chromia templates by substitution for Cr atoms at the surface of chromia [18]. Our calculations

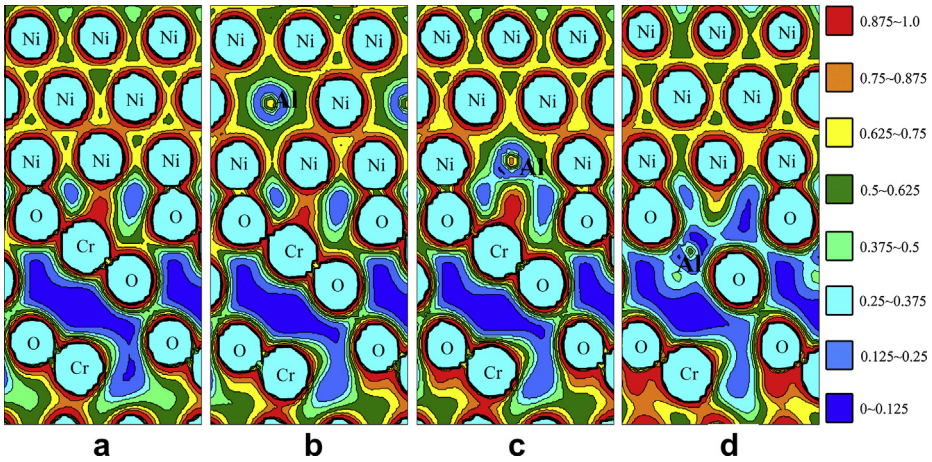

Fig. 4. Valence electron density distribution of the Ni/Cr_2O_3 interface with the Al atom at different diffusion sites: (a) clean interface, (b) Al atom in Ni bulk, (c) Al atom on the interface, and (d) Al atom in Cr_2O_3 bulk.

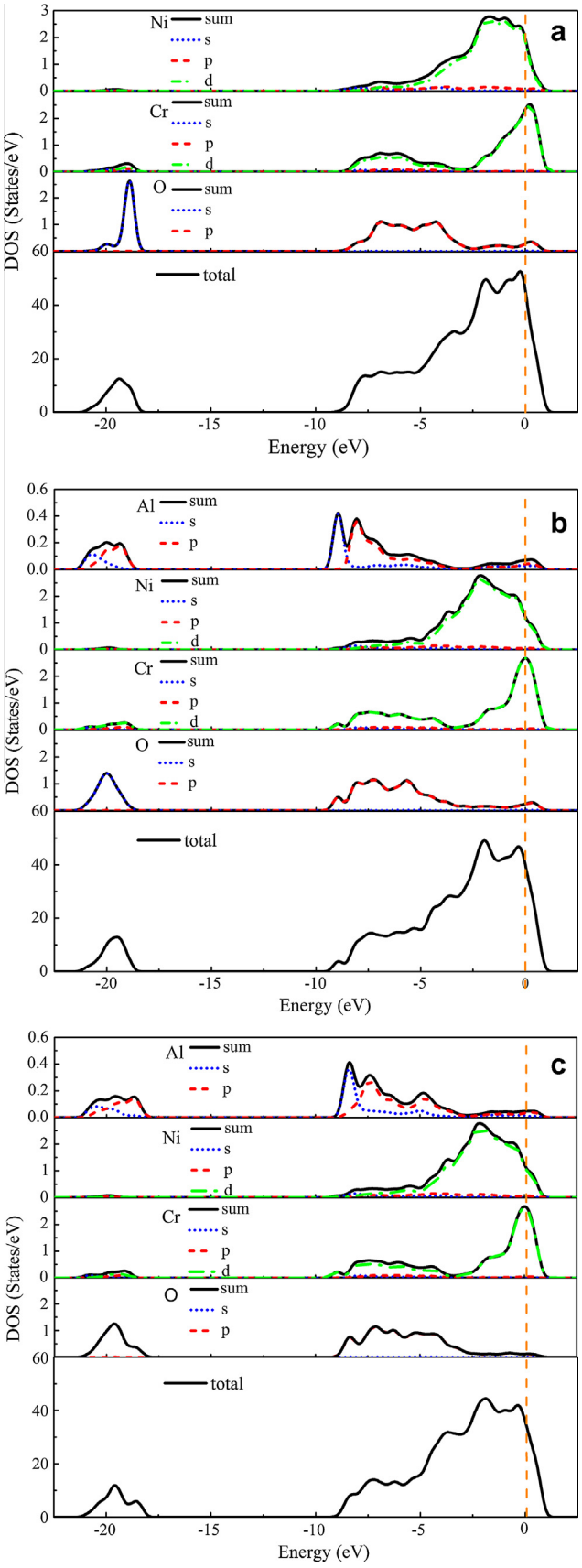

Fig. 5. Density of states of the interfaces with different Al coverage: (a) clean interface, (b) 50% Al coverage, and (c) 100% Al coverage.

represent further evidence for the experimentally observed behavior.

3.4. Analysis of electronic structure

The mechanical strength of the interface is unavoidably determined by the atomic bonding strength. Thus it is necessary to investigate the electronic structure and bonding nature of the interface between Ni and Cr_2O_3. Therefore we used the charge density distribution, the density of states (DOS) and Mulliken population to investigate the interfacial electron properties and the effect of aluminum on the interfacial structures.

Revealing pictures emerged from a comparison of the charge densities with the Al atom at different diffusion positions are shown in Fig. 4. To simulate the diffusion of aluminum, we started with the clean 'top-O' interface as the initial structure (Fig. 4a). And Fig. 4b–d represents to the electron density of the interface with aluminum at different diffusion sites, respectively. In Fig. 4a–d, although the influences of Al atom exist, we can find a remarkable charge overlap between the interfacial Ni and O atoms in each model, which indicates the formation of strong Ni-3d/O-2p orbital hybridization. Note that when the Al atom is firmed in Ni bulk (Fig. 4b), the strong ionic Ni–Al bonds can improve the strength. The electron charge density contours (Fig. 4c) suggests that the drastic promotion in adhesion may be ascribed to the strong Al bonding to O atoms across the interface, corresponding to the increment of "bond density". We can see that the substitution of Al atom for Cr atom is beneficial to bonding between Al and Ni atoms, as shown in (Fig. 4d), and that the newly-formed cross-interface bonds are probably responsible for the enhanced adhesion compared to the clean interface. This increment is also proved by comparing the interlayer distances of clean interface and those of construction with an Al substituting for Cr atom. For the clean one, the interfacial distance between Ni and O layer is 0.116 Å, while it shrinks to 0.104 Å with the appearance of aluminum.

DOS and partial DOS (PDOS) analysis of the effect of Al atoms on Ni/Cr_2O_3 interface are shown in Fig. 5. For the clean Ni/Cr_2O_3 interface, we can clearly see the range from −9.5 eV to 1.5 eV is filled by valence electrons. In addition, there are some charge in the region ranging from −21.5 eV to −17.9 eV mainly dominated by O-2p and Cr-3d orbital. Devoted by Ni-3d, Cr-3d and O-2s charge, the clean interface has the strongest peak (52.7 states/eV) at −0.2 eV, resulting in the value (46.3 states/eV) of the DOS at the Fermi energy. For the case with 50% Al coverage, the range filled by valence charge shifts downward in energy. Because of the participation of Al atom, there is a resonance with the formation of the polar covalent bond between aluminum and oxygen atoms in the region from −21.8 eV to −18.2 eV, which is consistent with our results of charge density. In the same way, a new peak emerges at −8.9 eV as a consequence of the resonance between aluminum and oxygen. It is necessary to note that the most distinct difference between the clean interface and the interface with 50% Al coverage is the position and shape of the strongest peak. By comparing with the DOS of clean interface, the strongest peak (49.1 states/eV) shifts to lower energy (−2.0 eV) and become mild, following with the decrease of value at the Fermi level (40.1 states/eV). Furthermore, with 100% Al coverage the band occupied by the valence electrons slightly removes downward in energy again. In the region from −21.6 eV to −17.6 eV, due to the drastic reactions between Al atoms and O atoms, the spectra are widening, with the original peak splitting into two parts. Contrasted with 50% Al covered case, the new peak become more intensive at −8.3 eV and the strongest peak (44.5 states/eV) is dropped down again. With the increase of Al coverage, the number of eigenstates at Fermi level is reduced from 40.1 states/eV to 35.5 states/eV.

Table 3
Atomic charges on the Ni, O, Cr and Al atoms close to the interfaces calculated from Mulliken population analysis.

Clean interface			50% Al coverage			100% Al coverage		
Atom	Total electron (e)	Transfer charge (e)	Atom	Total electron (e)	Transfer charge (e)	Atom	Total electron (e)	Transfer charge (e)
Ni	10.00	0.00	Ni	9.86	0.14	Cr	13.92	0.08
Ni	10.02	−0.02	Ni	9.92	0.08	Ni	9.83	0.17
Ni	9.81	0.19	Ni	9.75	0.25	Cr	13.82	0.18
Ni	9.91	0.09	Cr	13.93	0.07	Ni	9.89	0.11
O	6.50	−0.50	O	6.55	−0.55	O	6.63	−0.63
O	6.45	−0.45	O	6.66	−0.66	O	6.76	−0.76
O	6.46	−0.46	O	6.64	−0.64	O	6.87	−0.87
Cr	13.16	0.84	Al	1.45	1.55	Al	1.48	1.52
Cr	13.23	0.77	Cr	13.19	0.81	Al	1.52	1.48
O	6.51	−0.51	O	6.65	−0.65	O	6.76	−0.76
O	6.49	−0.49	O	6.69	−0.69	O	6.81	−0.81
O	6.49	−0.49	O	6.67	−0.67	O	6.76	−0.76
Species	Average transfer charge (e)		Species	Average transfer charge (e)		Species	Average transfer charge (e)	
O	−0.4811		O	−0.5911		O	−0.6667	
Cr	0.6617		Cr	0.5233		Cr	0.415	
Ni	0.021		Ni	0.04		Ni	0.0364	
–	–		Al	1.55		Al	1.5	

As shown in Fig. 5a–c, we can safely conclude that, with the presence of aluminums, sharp peaks in the total density of states become mild, and Al atoms also have the significant influence on the charge distribution of Ni, Cr and O. Compared with the clean interface, the pronounced difference is that, with increase of Al coverage, the states shift to low energy region at a large extent, which indicates that the stability of construction is improved. In fact, that is to say, the most stable structure is the three-layer Ni/Al_2O_3/Cr_2O_3 oxide. That is consistent with our previous calculation.

Although a DOS analysis can reveal valuable information about the nature of covalent bonding, it provides limited insight into matters related to charge transfer. But such data are important for understanding the character of interfacial bonding. A common tool used to provide a semi-quantitative measurement of charge transfer is Mulliken population analysis [36]. Table 3 indicates atomic population for clean interface and interface with 50%, 100% Al coverage, respectively. It lists the charges on the interfacial Ni and Cr(Al) atoms, and the O atoms close to the substituted Cr atoms, which have great changes with the presence of Al atoms. We found that for the clean interface, the transfer charges of the two Cr atoms are 0.84 and 0.77, while those of Cr and Al atom, when an Al atom presents to represent Cr, increase to 1.55 and 0.81. Finally, the transfer charges originating from Al atoms turn into 1.52 and 1.48 with the addition of Al coverage. The trend indicates that the increasing number of diffused Al atoms engender a powerful positive electricity field, followed with the adding attraction for oxygen anion, as we all known, which is acting as an acceptor. This conjecture can be proved by higher electronegativity of the six oxygen atoms being next to aluminum. This conclusion is consistent with the phenomenon in the experiments, revealing that the oxygen concentration caused by Al diffusion at Ni/Cr_2O_3 contributes to the formation of Ni/Al_2O_3/Cr_2O_3. The average values indicate the effects of Al coverage on the transfer charge of Ni, Cr and O atoms. Besides these results, the electrical nature of replaced Cr atoms in the bulk Ni part is similar to that of Ni atoms, indicating the existence of metallic bonding. The normal valence of Ni, O, Cr are +2, −2, +3, whereas the obtained absolute value about charge of the interfacial atoms are lower, and this difference is related to the formation of ionic–covalent bonds at the interfaces, in good agreement with the charge density map.

4. Conclusions

In summary, a plane-wave pseudopotential based DFT method is employed to study the properties of Ni(111)/Cr_2O_3(0001) interface and the diffusion of aluminum at the Ni(111)/Cr_2O_3(0001) interface. For the (0001) surface of Cr_2O_3, O-terminated surface has a very unfavorable energy while Cr-terminated Cr_2O_3(0001) surface is surprisingly stable. However, the results showed that interface formation with Ni can in fact reverse the relative stability of O-terminated and Cr-terminated interface. Through Ni–O covalent–ionic bonds, the enhanced interfacial bonding strength with larger work of adhesion indicates the O-terminated Ni(111)/Cr_2O_3(0001) interfaces are more stable than Cr-terminated ones. The discussion of aluminum diffusion hinted that Al atoms in Ni slab would diffuse into Cr_2O_3 slab through the Ni/Cr_2O_3 and occupy Cr-substitutional sites. The structural stability of Ni/Al_2O_3/Cr_2O_3 was higher than that of Ni/Cr_2O_3.

Acknowledgements

The authors would like to gratefully acknowledge the support of the National Natural Science Foundation of China (Grant No. 50874079) and the Shanxi Outstanding Graduate Innovation Project (Grant No. 02100331).

References

[1] V.P. Deodeshmukh, S.J. Matthews, D.D. Klarstrom, Int. J. Hydrogen Energy 36 (2011) 4580–4587.
[2] L. Hu, D. Hovis, A.H. Heuer, Scr. Mater. 61 (2009) 157–160.
[3] G.Y. Liang, C. Zhu, X.Y. Wu, Y. Wu, Appl. Surf. Sci. 257 (2011) 6468–6473.
[4] L. Marchetti, S. Perrin, Y. Wouters, M. Pijolat, Electrochim. Acta 55 (2010) 5384–5392.
[5] Wenjun Kuang, Xingiang Wu, En-Hou Han, Jiancun Rao, Corros. Sci. 53 (2011) 3853–3860.
[6] L. Hu, D.B. Hovis, A.H. Heuer, Oxid. Met. 73 (2010) 275–288.
[7] C.S. Gigins, F.S. Pettit, J. Electrochem. Soc. 118 (1971) 1782–1790.
[8] T.J. Nijdam, L.P.H. Jeurgens, W.G. Sloof, Acta Mater. 53 (2005) 1643–1653.
[9] G. Brewster, N. D'souza, K.S. Ryder, S. Simmonds, H.B. Dong, Metall. Mater. Trans. A 43A (2012) 1288–1302.
[10] S.V. Eremeev, S. Schmauder, S. Hocker, S.E. Kulkova, Physica B 404 (2009) 2065–2071.
[11] W. Zhang, J.R. Smith, A.G. Evans, Acta Mater. 50 (2002) 3803–3816.
[12] Siqi Shi, Shingo Tanaka, Masanori Kohhyama, Phys. Rev. B 76 (2007) 075431.
[13] X.G. Wang, J.R. Smith, A.G. Evans, Phys. Rev. B 74 (2006) 081403.
[14] M.X. Xiao, M. Zhao, X.Y. Lang, Y.F. Zhu, Q. Jiang, Chem. Phys. Lett. 542 (2012) 85–88.
[15] Isil Ozfidan, Kuiying Chen, Ming Fu, Metall. Mater. Trans. A 42A (2011) 4126–4136.
[16] Tian Zhang, Hongbo Guo, Shengkai Gong, Huibin Xu, Corros. Sci. 66 (2013) 59–66.
[17] F. Zuliani, R. Choudhury, O. Sbaizero, A. De Vita, Acta Mater. 55 (2007) 5813–5821.
[18] Jizhong Sun, Thomas Stirner, Thin Solid Films 517 (2009) 5512–5515.
[19] P.D. Han, H.F. Li, X.L. Sun, W. Liang, H.B. Dong, B.S. Xu, Ironmak. Steelmak. 38 (2011) 530–533.

[20] N. Troullier, J.L. Martins, Phys. Rev. B 43 (1991) 1993–2006.
[21] J.P. Perdew, A. Zunger, Phys. Rev. B 23 (1981) 5048–5079.
[22] D.M. Ceperley, B.J. Alder, Phys. Rev. Lett. 45 (1980) 566.
[23] H. Monkhorst, J.D. Pack, Phys. Rev. B 13 (1976) 5188–5192.
[24] Suchismita Sanyal, Umesh V. Waghmare, Timothy Hanlon, Ernest L. Hall, Mater. Sci. Eng. A 530 (2011) 373–377.
[25] M. Kresch, O. Delaire, R. Stevens, J.Y.Y. Lin, B. Fultz, Phys. Rev. B 75 (2007) 104301.
[26] A. Rohrbach, J. Hafner, G. Kresse, Phys. Rev. B 70 (2004) 125426.
[27] Jizhong Sun, Surf. Coat. Technol. 201 (2006) 4205–4208.
[28] A.L. Wysocki, Phys. Rev. B 86 (2012) 165443.
[29] Xiaogang Wang, Anne Chaka, Matthias Scheffler, Phys. Rev. Lett. 84 (2000) 3650–3653.
[30] W. Zhang, J.R. Smith, Phys. Rev. B 61 (2000) 16883–16889.
[31] M. Aldén, S. Mirbt, H.L. Skriver, N.M. Rosengaard, B. Johansson, Phys. Rev. B 46 (1992) 6303–6312.
[32] W.R. Tyson, W.A. Miller, Surf. Sci. 62 (1977) 267–276.
[33] H. Wawra, Z. Metallkd. 66 (1975) 395–401.
[34] A. Hashiban, C. Elsässer, M. Rühle, Acta Mater. 53 (2005) 5323–5332.
[35] G. Cantele, Phys. Rev. B 72 (2005) 113303.
[36] M.D. Segall, R. Shah, C.J. Pickard, M.C. Payne, Phys. Rev. B 54 (1996) 16317–16320.